Attaching Gold and Platinum to the Rim of Pyrene: A Synthetic and Spectroscopic Study

Wendy Yuqing Heng, Jian Hu, and John H. K. Yip*

Department of Chemistry, National University of Singapore, 3 Science Drive 3, Singapore 117543

Received July 18, 2007

A series of pyrenyl complexes containing one or two $AuPPh_3$ or $Pt(PEt_3)_2Br$ groups have been synthesized to probe the effects of metal on the absorption and emission properties of the organic molecule. The absorption spectra of the complexes showed perturbation of the metal centers on the pyrenyl ring, as manifested by a red shift of the $\pi \rightarrow \pi^*$ transitions of pyrene and intensification of the forbidden ^1L_b band. The perturbation increased with the number of metal ions attached to the pyrenyl ring. The Pt ion was stronger than the Au ion in perturbing the electronic structure of the pyrenyl ring. All pyrenyl complexes displayed fluorescence and phosphorescence in degassed solutions. The heavy-atom effect of the metal ions enhanced the phosphorescence. The quantum yield of phosphorescence was sensitive to the positions of metalation.

Introduction

Alternant aromatic hydrocarbons (AAH) are an important class of chromophores, including molecules such as benzene, naphthalene, anthracene, and pyrene.[1] These organic molecules, all displaying intense $\pi \rightarrow \pi^*$ transitions in the UV and/or visible region, occupy a central position in spectroscopy, photophysics, photochemistry, and bonding theory.[2] Although the effects of substituents on the electronic structures of AAH have been intensively investigated,[2,3] most of the works have focused on conventional substituents such as alkyls, amines, and halides and corresponding studies on the effects of metals have been rather limited. The electronic absorption and emission spectroscopy of metalated AAH should provide insights into the interactions between the metal and the extensive π-conjugated systems, the knowledge of which is crucial to developing this class of molecules into new organometallic functional materials. Because of strong exchange interaction, the singlet and triplet states of AAH are widely separated and the phosphorescence of highly conjugated AAH could occur in the near-infrared region. However, the intersystem crossing from the fluorescing singlet excited state to its corresponding phosphorescing triplet state is slow because of the unfavorable Franck–Condon factor due to the large singlet–triplet gap.[2,4] The third-row transition metals are known to increase the rate of intersystem crossing between the singlet and triplet excited states of organic molecules in a phenomenon known as the *heavy atom effect*, and this has the potential to enhance $^3\pi\pi^*$ phosphorescence of the compounds.[2a–c,4,5] This property of metalated AAH could be harnessed to create new near-infrared emitting materials.

As part of our ongoing effort to develop the coordination chemistry of AAH-based ligands,[6] we explored the possibility of using pyrene as a *multidentate* ligand in synthesizing polymetallic complexes. Pyrene has rich photophysical properties,[4,7] and it has been invoked in building luminescent metal complexes as part of the ligands.[8] However, organometallic complexes of pyrene are fewer by comparison. In most cases, the complexes of pyrene are the so-called π-complexes in which the metal center is attached to the ring via the π-bonding system.[9] To the best of our knowledge, only five σ-bonded organometallic pyrene complexes have been reported, which contain Ru(II),[8g]

* To whom correspondence should be addressed. E-mail: chmyiphk@nus.edu.sg.

(1) (a) Harvey, R. G. *Polycyclic Aromatic Hydrocarbons*; Wiley-VCH: New York, 1997. (b) Platt, J. R. *J. Chem. Phys.* **1949**, *17*, 484. (c) Michl, J. *Tetrahedron* **1984**, *40*, 3845.

(2) (a) Kessinger, M.; Michl, J. *Excited States and Photochemistry of Organic Molecules*; Wiley-VCH: New York, 1995. (b) Suzuki, H. *Electronic Absorption Spectra, and Geometry of Organic Molecules; an Application of Molecular Orbital Theory*; Academic Press: New York, 1967. (c) Turro, N. J. *Modern Molecular Photochemistry*; Benjamin: Menlo Park, NJ, 1978. (d) Dewar, M. J. S. *The Molecular Orbital Theory of Organic Chemistry*; McGraw-Hill: New York, 1969.

(3) (a) Reference 2a, pp 104–117. (b) Longuet-Higgins, H. C.; Coulson, C. A. *J. Chem. Soc.* **1949**, 971. (c) Vasak, M.; Whipple, M. R.; Berg, A.; Michl, J. *J. Am. Chem. Soc.* **1978**, *100*, 6872. (d) Steiner, R. P.; Michl, J. *J. Am. Chem. Soc.* **1978**, *100*, 6861.

(4) Birks, J. B. *Photophysics of Aromatic Molecules*; Wiley: London, 1970.

(5) (a) McClure, D. S. *J. Chem. Phys.* **1952**, *20*, 682. (b) Haskins-Glusac, K.; Ghiviriga, I.; Abboud, K. A.; Schanze, K. S. *J. Phys. Chem. B* **2004**, *108*, 4969. (c) Che, C.-M.; Chao, H.-Y.; Miskowski, V. M.; Li, Y.; Cheung, K.-K. *J. Am. Chem. Soc.* **2001**, *123*, 4985. (d) Chao, H.-Y.; Lu, W.; Li, Y.; Chan, M. C. W.; Che, C.-M.; Cheung, K.-K.; Zhu, N. *J. Am. Chem. Soc.* **2002**, *124*, 14696. (e) Osawa, M.; Hoshino, M.; Akita, M.; Wada, T. *Inorg. Chem.* **2005**, *44*, 1157. (f) Burress, C.; Elbjeirami, O.; Omary, M. A.; Gabbai, F. P. *J. Am. Chem. Soc.* **2005**, *127*, 12166. (g) Elbjeirami, O.; Burress, C. N.; Gabbai, F. P.; Omary, M. A. *J. Phys. Chem. C* **2007**, *111*, 9522. (h) Omary, M. A.; Kassab, R. M.; Haneline, M. R.; Elbjeirami, O.; Gabbai, F. P. *Inorg. Chem.* **2003**, *42*, 2176. (i) Mohamed, A. A.; Rawashdeh-Omary, M. A.; Omary, M. A.; Fackler, J. P., Jr *Dalton Trans.* **2005**, 2597.

(6) (a) Yip, J. H. K; Prabhavathy, J. *Angew. Chem., Int. Ed.* **2001**, *40*, 2159. (b) Lin, R.; Yip, J. H. K.; Zhang, K.; Koh, L. L.; Wong, K.-Y.; Ho, K. P. *J. Am. Chem. Soc.* **2004**, *126*, 15852. (c) Zhang, K.; Prabhavathy, J.; Yip, J. H. K.; Koh, L. L.; Tan, G. K.; Vittal, J. J. *J. Am. Chem. Soc.* **2003**, *125*, 8452. (d) Lin, R.; Yip, J. H. K. *Inorg. Chem.* **2006**, *45*, 4423.

(7) (a) Förster, T.; Kasper, K. *Z. Electrochem.* **1955**, *59*, 976. (b) Parker, C. A. *Adv. Photochem.* **1964**, *2*, 306.

(8) (a) Wilson, G. J.; Launikonis, A.; Sasse, W. H. F.; Mau, A. W.-H. *J. Phys. Chem. A* **1997**, *101*, 4860. (b) Tyson, D. S.; Castellano, F. N. *J. Phys. Chem. A* **1999**, *103*, 10955. (c) Juris, A.; Prodi, A. *New J. Chem.* **2001**, *25*, 1132. (d) Indelli, M. T.; Ghirotti, M.; Prodi, A.; Chiorboli, C.; Scandola, F.; McClenaghan, N. D.; Puntoriero, F.; Campagna, S. *Inorg. Chem.* **2003**, *42*, 5489. (e) Pomestchenko, I. E.; Luman, C. R.; Hissler, M.; Ziessel, R.; Castellano, F. N. *Inorg. Chem.* **2003**, *42*, 1394. (f) Tao, C.-H.; Zhu, N.; Yam, V. W.-W. *Chem. Eur. J.* **2005**, *11*, 1647. (g) Bonnefous, C.; Chouai, A.; Thummel, R. P. *Inorg. Chem.* **2001**, *40*, 5851. (h) Byrnes, M. J.; Chisholm, M. H.; Gallucci, J. A.; Liu, Y.; Ramnauth, R.; Turro, C. *J. Am. Chem. Soc.* **2005**, *127*, 17343.

10.1021/om700716p CCC: $37.00
Publication on Web 12/07/2007

Scheme 1

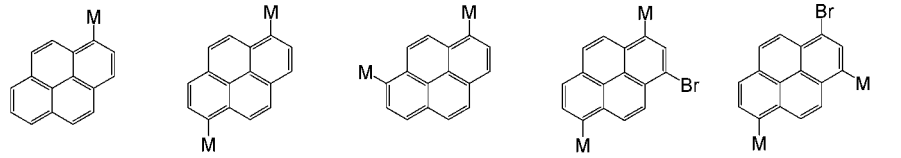

M = $AuPPh_3$ (**1**) M = $AuPPh_3$ (**2**) M = $AuPPh_3$ (**3**) M = $AuPPh_3$ (**4**) M = $Pt(PEt_3)_2Br$ (**9**)

= $Pt(PEt_3)_2Br$ (**5**) = $Pt(PEt_3)_2Br$ (**6**) = $Pt(PEt_3)_2Br$ (**7**) = $Pt(PEt_3)_2Br$ (**8**)

Pd(II),[10a] Ir(III),[10a] Pt(II),[10b] and Au(I)[10c] ions. A fundamental question we attempted to address is about the effects of a heavy metal on the absorption and emission properties of pyrene when it is attached to the ring via a σ-bond.[11] Herein we present the synthesis, characterization, and an investigation of the effect of the number and position of substitution on the electronic absorption spectrum and photophysical properties of a series of gold(I) and platinum(II) σ-bonded complexes with pyrene (Scheme 1). Che[12] and Yam[10c] have separately demonstrated the luminescence of arylgold(I) complexes. Our study showed that the metal ions can strongly perturb the pyrenyl ring, and interestingly the number and position of the metal ions play important roles in modulating the electronic structure of the organic moiety.

The initial advancement of arylgold(I) chemistry was largely limited to simple aromatics such as phenyl and its polyfluoroaryl derivatives,[13] but it has been extended to more elaborated aromatics such as vinylbenzene,[14a] biphenyl,[14b] and anthracene.[14c] The complexes were usually prepared by metathesis between the gold halides LAuX and standard aryl transferring reagents such as Grignard reagents, organolithium, organothallium, and organomercury compounds (L = phosphines, isocyanides, arsine, carbenes; X = halides).[13a–j] A convenient entry route into arylplatinum chemistry is through the oxidative addition of $Pt(PEt_3)_4$ to bromopolyaromatic molecules.[15] This method was used to prepare the platinated pyrenes in this work.

Experimental Section

General Methods. The syntheses of all metal complexes were carried out under N_2 by using standard Schlenck techniques. All solvents used in syntheses and spectroscopic measurements were purified according to standard methods. *n*-butyllithium (1.6 mol dm^{-3} in hexane) was obtained from Sigma-Aldrich and was titrated before used. $Au(PPh_3)Cl$,[16] $Pt(PEt_3)_4$,[17] 1-bromopyrene[18] and 1,3,6-tribromopyrene[19] were prepared according to literature procedures.

Physical Methods. ^1H and $^{31}P\{^1H\}$ NMR spectra were recorded on a Bruker ACF300 or AMX500 spectrometer, with ^1H chemical shifts (δ) given in ppm relative to residual nondeuterated $CDCl_3$ (δ 7.26). $^{31}P\{^1H\}$ chemical shifts were reported relative to external 85% aqueous H_3PO_4 (δ 0.0). Positive electrospray ionization (ESI) mass spectra were obtained with a Finnigan MAT 731 LCQ spectrometer. Electronic absorption and emission spectra were recorded by a Shimadzu UV-1601 spectrophotometer and a Perkin-Elmer LS50B luminescence spectrometer, respectively. The excitation wavelength used for all emission measurements was 320 nm. All solutions used for luminescence measurements were degassed with at least four freeze–pump–thaw cycles. Emission quantum yields were calculated with anthracene as a standard. Elemental analyses were carried out by the Elemental Analysis Laboratory, Department of Chemistry, National University of Singapore.

Synthesis. 1,6- and 1,8-Dibromopyrene. These compounds were prepared by double bromination of pyrene according to a similar literature method for the preparation of 1-brompyrene.[18] Pyrene (10.10 g, 0.050 mol) was dissolved in a mixture of Et_2O (200 mL) and CH_3OH (200 mL). HBr solution (48%, 12.45 mL, 0.110 mol) was then added to the solution. To this mixture was added dropwise H_2O_2 (30%, 10.30 mL, 0.100 mol) over 20 min. The resulting pale yellow slurry was stirred for 12 h. The product was filtered and washed with hot EtOH (50 mL). The ^1H NMR spectrum showed that the major products (>95%) were 1,6- and 1,8-dibromopyrene in an approximate ratio of 1:1. The two isomers were separated by fractional recrystallization from $CHCl_3$. Yield: 16.60 g, 92%.

1-Au(PPh_3)pyrene (1). To a stirred solution of 1-bromopyrene (0.639 g, 2.27 mmol) in freshly distilled Et_2O (30 mL) at 0 °C was added a solution of *n*-butyllithium in hexane (1.42 mL, 2.27 mmol).

(9) Some example of metal−pyrene π-complexes: (a) Hasegawa, T.; Sekine, M.; Schaefer, W. P.; Taube, H. *Inorg. Chem.* **1991**, *30*, 449. (b) Reingold, J. A.; Virkaitis, K. L.; Carpenter, G. B.; Sun, S.; Sweigart, D. A.; Czech, P. T.; Overly, K. R. *J. Am. Chem. Soc.* **2005**, *127*, 11146. (c) Morrison, W. H., Jr.; Ho, E. Y.; Hendrickson, D. N. *J. Am. Chem. Soc.* **1974**, *96*, 3603. (d) Munakata, M.; Wu, L. P.; Kuroda-Sowa, T.; Maekawa, M.; Suenaga, Y.; Sugimoto, K. *Inorg. Chem.* **1997**, *36*, 4903.

(10) (a) Ionkin, A. S.; Marshall, W. J.; Fish, B. M. *Organometallics* **2006**, *25*, 1461. (b) Weisemann, C.; Schmidtberg, G.; Brune, H.-A. *J. Organomet. Chem.* **1989**, *365*, 403. (c) Yam, V. W.-W.; Choi, S. W.-K.; Cheung, K.-K. *J. Chem. Soc., Dalton Trans.* **1996**, 3411.

(11) During the preparation of this paper, Gray et al. reported the syntheses and photophysics of two mononuclear gold(I)−pyrenyl complexes with carbene and $P(Cy)_3$ligands: Partyka, D. V.; Esswein, A. J.; Zeller, M.; Hunter, A. D.; Gray, T. G. *Organometallics* **2007**, *26*, 3279.

(12) Hong, X.; Cheung, K.-K.; Guo, C.-X.; Che, C.-M. *J. Chem. Soc., Dalton Trans.* **1994**, 1867.

(13) (a) Usón, R.; Laguna, A. *Coord. Chem. Rev.* **1986**, *70*, 1. (b) Schmidbaur, H. *Gold Progress in Chemistry, Biochemistry and Technology*; Wiley: Chichester, U.K., 1999; p 648. (c) Calvin, G.; Coates, G. E.; Dixon, P. E. *Chem. Ind.* **1959**, 1628. (d) Coates, G. E.; Parkin, G. *J. Chem. Soc.* **1962**, 3220. (e) Vaughan, L. G.; Sheppard, W. A. *J. Am. Chem. Soc.* **1969**, *91*, 6161. (f) Usón, R.; Laguna, A.; Buil, L. *J. Organomet. Chem.* **1975**, *85*, 403. (g) Usón, R.; Laguna, A.; Brun, P. *J. Organomet. Chem.* **1979**, *182*, 449. (h) Porter, K. A.; Schier, A.; Schmidbaur, H. *Organometallics* **2003**, *22*, 4922. (i) Laguna, A.; Laguna, M.; Gimeno, M. C.; Jones, P. G. *Organometallics* **1992**, *11*, 2759. (j) Bardají, M.; Jones, P. G.; Laguna, A.; Moracho, A.; Fischer, A. K. *J. Organomet. Chem.* **2002**, *648*, 1. (k) Sladek, A.; Hofreiter, S.; Paul, M.; Schmidbaur, H. *J. Organomet. Chem.* **1995**, *501*, 47.

(14) (a) Croix, C.; Balland-Longeau, A.; Allouchi, H.; Giorgi, M.; Duchêne, A.; Thibonnet, J. *J. Organomet. Chem.* **2005**, *690*, 4835. (b) Porter, K. A.; Schier, A.; Schmidbaur, H. *Perspect. Organomet. Chem.* **2002**, 74. (c) Yam, V. W.-W.; Cheung, K.-L.; Yip, S.-K.; Zhu, N. *Photochem. Photobiol. Sci.* **2005**, *4*, 149.

(15) (a) Singh, A.; Sharp, P. R. *J. Am. Chem. Soc.* **2006**, *128*, 5998. (b) Lucassen, A. C. B.; Shimon, L. J. W.; van der Boom, M. E. *Organometallics* **2006**, *25*, 3308. (c) Strawser, D.; Karton, A.; Zenkina, O. V.; Iron, M. A.; Shimon, L. J. W.; Martin, J. M. L.; van der Boom, M. E. *J. Am. Chem. Soc.* **2005**, *127*, 9322. (d) Kim, D.; Paek, J. H.; Jun, M.-J.; Lee, J. Y.; Kang, S. O.; Ko, J. *Inorg. Chem.* **2005**, *44*, 7886. (e) Lee, H. B.; Sharp, P. R. *Organometallics* **2005**, *24*, 4875. (f) Kryschenko, Y. K.; Seidel, S. R.; Muddiman, D. C.; Nepomuceno, A. I.; Stang, P. J. *J. Am. Chem. Soc.* **2003**, *125*, 9647. (g) Chantson, J. T.; Lotz, S.; Ichharam, V. *New J. Chem.* **2003**, *27*, 1735. (h) Kryschenko, Y. K.; Seidel, S. R.; Arif, A. M.; Stang, P. J. *J. Am. Chem. Soc.* **2003**, *125*, 5193. (i) Manna, J.; Kuehl, C. J.; Whiteford, J. A.; Stang, P. J. *Organometallics* **1997**, *16*, 1897.

(16) Baenziger, N. C.; Bennett, W. E.; Soboroff, D. M. *Acta Crystallogr.* **1976**, *B32*, 962.

(17) Yoshida, T.; Matsuda, T.; Otsuka, S. *Inorg. Synth.* **1990**, *28*, 122.

(18) Vyas, P. V.; Bhatt, A. K.; Ramachandraiah, G.; Bedekar, A. V. *Tetrahedron Lett.* **2003**, *44*, 4085.

(19) (a) Maeda, H.; Maeda, T.; Mizuno, K.; Fujimoto, K.; Shimizu, H.; Inouye, M. *Chem. Eur. J.* **2006**, *12*, 824–831. (b) Vollmann, H.; Becker, H.; Correll, M.; Streeck, H. *Justus Liebigs Ann. Chem.* **1937**, *531*, 1.

After 10 min, $Au(PPh_3)Cl$ (1.124 g, 2.27 mmol) was added to the resulting orange-yellow suspension and the mixture was warmed to room temperature. After this mixture was stirred for 2 h, 20 mL of CH_2Cl_2 was added to the orange suspension and the mixture was filtered. The filtrate was then concentrated, and hexane (100 mL) was added to precipitate the product as pale beige solids. Recrystallization by layering of hexane onto a CH_2Cl_2 solution of the solid afforded the product as orange-yellow crystals. Yield: 0.80 g, 53%. Anal. Calcd for $C_{34}H_{24}AuP \cdot 0.25CH_2Cl_2$: C, 60.34; H, 3.62. Found: C, 60.05; H, 3.64. ^{1}H NMR ($CDCl_3$, 500 MHz): δ 8.78 (d, 1H, $^3J_{H10-H9}$ = 8.8 Hz, H_{10}), 8.33 (dd, 1H, $^3J_{H2-H3}$ = 7.4 Hz, $^4J_{HP}$ = 5.3 Hz, H_2), 8.14 (d, 1H, $^3J_{H3-H2}$ = 7.4 Hz, H_3), 8.08 (m, 2H, $H_{6,8}$), 8.03 (d, 1H, $^3J_{H4-H5}$ = 8.9 Hz, $H_{4/5}$), 8.01 (d, 1H, $^3J_{H4-H5}$ = 8.9 Hz, $H_{4/5}$), 7.95 (d, 1H, $^3J_{H9-H10}$ = 8.8 Hz, H_9), 7.94–7.91 (m, 1H, H_7), 7.74–7.70 (m, 6H, Ph), 7.54–7.52 (m, 9H, Ph). ^{31}P{^{1}H} NMR ($CDCl_3$, 121.5 MHz): δ 44.85 (s). ESI-MS (*m*/*z*): 660.0 $[M]^+$.

1,6-Bis[Au(PPh$_3$)]pyrene (2). The procedure used was similar to that for **1**, except that 1,6-dibromopyrene (0.471 g, 1.31 mmol) and 2 mol equiv of *n*-butyllithium (1.64 mL, 2.62 mmol) and $Au(PPh_3)Cl$ (1.296 g, 2.62 mmol) were used. Pale yellow crystals of the product were obtained from diffusion of Et_2O into a CH_2Cl_2 solution of the crude product. Yield: 1.19 g, 81%. Anal. Calcd for $C_{52}H_{38}Au_2P_2 \cdot CH_2Cl_2$: C, 52.89; H, 3.35. Found: C, 52.39; H, 3.65. ^{1}H NMR ($CDCl_3$, 300 MHz): δ 8.69 (d, 2H, $^3J_{H5-H4}$ = 9.0 Hz, $H_{5,10}$), 8.24 (dd, 2H, $^3J_{H2-H3}$ = 7.4 Hz, $^4J_{H-P}$ = 5.3 Hz, $H_{2,7}$), 8.05 (dd, 2H, $^3J_{H3-H2}$ = 7.4 Hz, $^5J_{H-P}$ = 1 Hz, $H_{3,8}$), 7.97 (d, 2H, $^3J_{H4-H5}$ = 9.0 Hz, $H_{4,9}$), 7.76–7.68 (m, 12H, Ph), 7.53–7.50 (m, 18H, Ph). ^{31}P{^{1}H} NMR ($CDCl_3$, 121.5 MHz): δ 45.00 (s). ESI-MS (*m*/*z*): 1118.9 $[M]^+$.

1,8-Bis[Au(PPh$_3$)]pyrene (3). The procedure used was same as that for **2**. except that 1,8-dibromopyrene (0.432 g, 1.20 mmol) and 2 mol equiv of *n*-butyllithium (1.50 mL, 2.40 mmol) and $Au(PPh_3)Cl$ (1.187 g, 2.40 mmol) were used in the reaction. Orange-yellow crystals of the product were obtained from layering of hexane onto a CH_2Cl_2 solution of the crude product. Yield: 0.80 g, 60%. Anal. Calcd for $C_{52}H_{38}Au_2P_2 \cdot CH_2Cl_2$: C, 52.89; H, 3.35. Found: C, 53.44; H, 3.41. ^{1}H NMR ($CDCl_3$, 300 MHz): δ 8.74 (s, 2H, $H_{9,10}$), 8.24 (dd, 2H, $^3J_{H2-H3}$ = 7.4 Hz, $^4J_{H-P}$ = 5.3 Hz, $H_{2,7}$), 8.05 (dd, 2H, $^3J_{H3-H2}$ = 7.4 Hz, $^5J_{H-P}$ = 1 Hz, $H_{3,6}$), 7.90 (s, 2H, $H_{4,5}$), 7.76–7.68 (m, 12H, Ph), 7.52–7.50 (m, 18H, Ph). ^{31}P{^{1}H} NMR ($CDCl_3$, 121.5 MHz): δ 44.95 (s). ESI-MS (*m*/*z*): 1118.9 $[M]^+$.

1,6-Bis[Au(PPh$_3$)]-3-bromopyrene (4). The procedure used was similar to that for **1**, except that 1,3,6-tribromopyrene (0.440 g, 1.00 mmol) and 3 mol equiv of *n*-butyllithium (1.95 mL, 3.12 mmol) and $Au(PPh_3)Cl$ (1.50 g, 3.03 mmol) were used in the reaction. Crystals of the product were obtained from Et_2O/CH_2Cl_2. Yield: 1.03 g, 86%. Anal. Calcd for $C_{52}H_{37}Au_2P_2Br$: C, 52.15; H, 3.11. Found: C, 52.26; H, 3.38. ^{1}H NMR ($CDCl_3$, 500 MHz): δ 8.79 (d, 1H, $^3J_{H5-H4}$ = 9.2 Hz, H_5), 8.64 (d, 1H, $^3J_{H10-H9}$ = 9.0 Hz, H_{10}), 8.50 (d, 1H, $^4J_{H-P}$ = 5.7 Hz, H_2), 8.33 (d, 1H, $^3J_{H4-H5}$= 9.2 Hz, H_4), 8.27 (dd, 1H, $^3J_{H7-H8}$= 7.5 Hz, $^4J_{H-P}$ = 5.3 Hz, H_7), 8.08 (dd, 1H, $^3J_{H8-H7}$= 7.5 Hz, $^5J_{H-P}$ = 1 Hz, H_8), 7.98 (d, 1H, $^3J_{H9-H10}$= 9.0 Hz, H_9), 7.74–7.69 (m, 12H, Ph), 7.53–7.50 (m, 18H, Ph). ^{31}P{^{1}H} NMR ($CDCl_3$, 202.4 MHz): δ 44.94 (s), 44.44 (s). ESI-MS (*m*/*z*): 1198.9 $[M]^+$.

1-[*trans*-Pt(PEt$_3$)$_2$Br]pyrene (5). To a solution of $Pt(PEt_3)_4$ (2.0 g, 3.0 mmol) in toluene (60 mL) was added 1-bromopyrene (0.765 g, 2.72 mmol). The reaction mixture was stirred for 18 h at room temperature, during which time an orange-yellow solution resulted. The solvent was then removed and the resultant pale yellow solid redissolved in a minimum volume of CH_2Cl_2. Cold hexane (150 mL) was added to precipitate out the product. Pale yellow crystals were obtained from diffusing hexane into a CH_2Cl_2 solution of the product. Yield: 1.57 g, 81%. Anal. Calcd for $C_{28}H_{39}PtP_2Br$: C, 47.20; H, 5.52. Found: C, 47.71; H, 5.64. ^{1}H NMR ($CDCl_3$, 300 MHz): δ 8.85 (d, 1H, $^3J_{H10-H9}$ = 9.0 Hz, H_{10}), 8.18 (d, 1H, $^3J_{H2-H3}$ = 7.9 Hz, $^3J_{HPt}$ = 69 Hz, H_2), 8.09 (m, 2H, $^3J_{H6,8-H7}$ = 7.6 Hz, $H_{6,8}$), 7.98–7.88 (m, 4H, $H_{4,5,7,9}$), 7.78 (d, 1H, $^3J_{H3-H2}$ = 7.9 Hz, H_3), 1.60–1.46 (m, 12H, PCH_2CH_3), 1.05–0.95 (m, 18H, PCH_2CH_3). ^{31}P{^{1}H} NMR ($CDCl_3$, 121.5 MHz): δ 12.63 (s, $^1J_{P-Pt}$ = 2700 Hz). ESI-MS (*m*/*z*): 631.1 $[M - Br]^+$.

1,6-Bis[*trans*-Pt(PEt$_3$)$_2$Br]pyrene (6). The procedure used was the same as that for **5**, except that 1,6-dibromopyrene (0.490 g, 1.36 mmol) and 2 mol equiv of $Pt(PEt_3)_4$ (2.0 g, 3.0 mmol) were used. Pale yellow crystals of the product were obtained from diffusing Et_2O into a CH_2Cl_2 solution of the crude product. Yield: 1.42 g, 85%. Anal. Calcd for $C_{40}H_{68}Pt_2P_4Br_2$: C, 39.29; H, 5.61. Found: C, 39.49; H, 5.76. ^{1}H NMR ($CDCl_3$, 300 MHz): δ 8.68 (d, 2H, $^3J_{H5-H4}$ = 9.0 Hz, $H_{5,10}$), 8.06 (d, 2H, $^3J_{H2-H3}$ = 7.8 Hz, $^3J_{H-Pt}$ = 65 Hz, $H_{2,7}$), 7.85 (d, 2H, $^3J_{H4-H5}$ = 9.0 Hz, $H_{4,9}$), 7.69 (d, 2H, $^3J_{H3-H2}$ = 7.8 Hz, $H_{3,8}$), 1.60–1.46 (m, 24H, PCH_2CH_3), 1.05–0.95 (m, 36H, PCH_2CH_3). ^{31}P{^{1}H} NMR ($CDCl_3$, 121.5 MHz): δ 12.66 (s, $^1J_{P-Pt}$ = 2720 Hz). ESI-MS (*m*/*z*): 1221.9 $[M]^+$, 1142.1 $[M - Br]^+$.

1,8-Bis[*trans*-Pt(PEt$_3$)$_2$Br]pyrene (7). This compound was prepared from $Pt(PEt_3)_4$ (2.0 g, 3.0 mmol) and 1,8-dibromopyrene (0.490 g, 1.36 mmol) by using the same procedure as for **6**. Recrystallization from vapor diffusion of Et_2O into a CH_2Cl_2 solution of the crude product afforded the product as pale orange-red crystals. Yield: 0.88 g, 53%. Anal. Calcd for $C_{40}H_{68}Pt_2P_4Br_2$: C, 39.29; H, 5.61. Found: C, 39.68; H, 5.73. ^{1}H NMR ($CDCl_3$, 300 MHz): δ 8.77 (s, 2H, $H_{5,10}$), 8.02 (d, 2H, $^3J_{H2-H3}$ = 7.7 Hz, $^3J_{H-Pt}$ = 70 Hz, $H_{2,7}$), 7.82 (s, 2H, $H_{4,9}$), 7.69 (d, 2H, $^3J_{H3-H2}$ = 7.7 Hz, $H_{3,8}$), 1.60–1.46 (m, 24H, PCH_2CH_3), 1.05–0.95 (m, 36H, PCH_2CH_3). ^{31}P{^{1}H} NMR ($CDCl_3$, 121.5 MHz): δ 12.30 (s, $^1J_{P-Pt}$ = 2730 Hz). ESI-MS (*m*/*z*): 1221.9 $[M]^+$.

1,6-Bis[*trans*-Pt(PEt$_3$)$_2$Br]-3-bromopyrene (8) and 1,8-Bis[*trans*-Pt(PEt$_3$)$_2$Br]-3-bromopyrene (9). To a solution of $Pt(PEt_3)_4$ (2.0 g, 3.0 mmol) in toluene (60 mL) was added 1,3,8-tribromopyrene (0.597 g, 1.36 mmol). The reaction mixture was stirred for 18 h, the solvent was then removed, and the resultant white solid was redissolved in a minimum volume of CH_2Cl_2. Hexane was slowly added to precipitate out the less soluble 1,6-bis[*trans*-$Pt(PEt_3)_2Br$]-3-bromopyrene as a beige solid, which was collected by suction filtration. Removal of solvent from the filtrate gave a beige solid containing 1,8-bis[*trans*-$Pt(PEt_3)_2Br$]-3-bromopyrene. Recrystallization from vapor diffusion of diethyl ether into a CH_2Cl_2 solution of the former solid afforded complex **8** as yellow crystals. Repeated recrystallizations from vapor diffusion of ether into a CH_2Cl_2 solution of the latter solid afforded complex **9** as pale orange-red crystals. Yield: 1.58 g, 45% for each isomer. Data for **8** are as follows. Anal. Calcd for $C_{40}H_{67}Pt_2P_4Br_3$: C, 36.91; H, 5.19. Found: C, 37.03; H, 5.36. ^{1}H NMR ($CDCl_3$, 300 MHz): δ 8.78 (d, 1H, $^3J_{H5-H4}$= 9.3 Hz, H_5), 8.68 (d, 1H, $^3J_{H10-H9}$ = 8.9 Hz, H_{10}), 8.34 (s, 1H, $^3J_{H-Pt}$ = 74 Hz, H_2), 8.19 (d, 1H, $^3J_{H4-H5}$ = 9.3 Hz, H_4), 8.12 (d, 1H, $^3J_{H7-H8}$ = 7.7 Hz, $^3J_{H-Pt}$ = 69 Hz, H_7), 7.88 (d, 1H, $^3J_{H9-H10}$ = 8.9 Hz, H_9), 7.72 (d, 1H, $^3J_{H8-H7}$ = 7.7 Hz, H_8), 1.60–1.45 (m, 24H, PCH_2CH_3), 1.06–0.97 (m, 36H, PCH_2CH_3). ^{31}P{^{1}H} NMR ($CDCl_3$, 121.5 MHz): δ 12.68 (s, 2P, $^1J_{P-Pt}$ = 2710 Hz), 12.25 (s, 2P $^1J_{P-Pt}$ = 2680 Hz). ESI-MS (*m*/*z*): 1301.8 $[M]^+$, 1223.1 $[M - Br]^+$. Data for **9** are as follows. Anal. Calcd for $C_{40}H_{67}Pt_2P_4Br_3$: C, 36.91; H, 5.19. Found: C, 37.13; H, 5.29. ^{1}H NMR ($CDCl_3$, 300 MHz): δ 8.84–8.75 (m, 2H, $H_{4,5}$), 8.31 (s, 1H, $^3J_{H-Pt}$ = 75 Hz, H_2), 8.19 (d, 1H, $^3J_{H10-H9}$ = 9.1 Hz, H_{10}), 8.07 (d, 1H, $^3J_{H7-H8}$ = 7.9 Hz, $^3J_{H-Pt}$ = 58 Hz, H_7), 7.92 (d, 1H, $^3J_{H9-H10}$ = 9.1 Hz, H_9), 7.74 (d, 1H, $^3J_{H8-H7}$ = 7.9 Hz, H_8), 1.60–1.45 (m, 24H, PCH_2CH_3), 1.05–0.93 (m, 36H, PCH_2CH_3). ^{31}P{^{1}H} NMR ($CDCl_3$, 121.5 MHz): δ 12.19 (s, 2P, $^1J_{P-Pt}$ = 2720 Hz), 11.92 (s, 2P, $^1J_{P-Pt}$ = 2680 Hz). ESI-MS (*m*/*z*): 1302.0 $[M]^+$, 1222.0 $[M - Br]^+$.

X-ray Crystallography. Single crystals of the compounds were mounted on a glass fiber and used for the diffraction experiments.

Table 1. Crystallographic Data of 1–8[a]

	1·0.5CH_2Cl_2	**2**·CH_2Cl_2	**3**·CH_2Cl_2	**4**·Et_2O	**5**	**6**	**7**	**8**
formula	$C_{34.5}H_{25}AuP$	$C_{53}H_{40}Au_2Cl_2P_2$	$C_{53}H_{40}Au_2Cl_2P_2$	$C_{56}H_{47}Au_2BrOP_2$	$C_{28}H_{39}BrP_2Pt$	$C_{40}H_{68}Br_2P_4Pt_2$	$C_{40}H_{68}Br_2P_4Pt_2$	$C_{40}H_{68}Br_3P_4Pt_2$
mol wt	702.93	1203.62	1203.62	1271.72	712.53	1222.82	1222.82	1302.73
temp (K)	243(2)	223(2)	223(2)	243(2)	223(2)	223(2)	223(2)	243(2)
cryst syst	monoclinic	triclinic	monoclinic	triclinic	monoclinic	monoclinic	orthorhombic	monoclinic
space group	$P2_1/c$	$P\bar{1}$	$P2_1/n$	$P\bar{1}$	$P2_1/c$	$P2_1/c$	$Pna2_1$	$P2_1/c$
a(Å)	12.030(2)	10.7417(6)	7.0423(6)	9.6714(5)	13.4514(6)	8.8737(5)	37.508(2)	9.0276(5)
b(Å)	15.178(3)	14.4354(7)	11.6307(10)	11.3463(6)	14.2834(6)	15.8737(9)	9.1892(6)	14.8358(8)
c(Å)	15.529(3)	15.7306(8)	55.107(5)	13.0570(7)	14.9128(7)	16.0938(9)	13.7163(9)	17.3662(9)
α (deg)	90	92.6170(10)	90	114.6030(10)	90	90	90	90
β (deg)	103.977(4)	103.0250(10)	90.598(2)	98.3000(10)	100.5680(10)	105.4020(10)	90	102.3620(10)
γ (deg)	90	111.3390(10)	90	97.5320(10)	90	90	90	90
V(Å^3)	2751.6(8)	2191.5(2)	4513.4(7)	1259.64(12)	2816.6(2)	2185.2(2)	4727.6(5)	2272.0(2)
Z	4	2	4	1	4	2	4	2
index ranges	$-14 \le h \le 15$, $-19 \le k \le 19$, $-13 \le l \le 20$	$-13 \le h \le 13$, $-18 \le k \le 18$, $-20 \le l \le 20$	$-8 \le h \le 7$, $-13 \le k \le 13$, $-60 \le l \le 65$	$-12 \le h \le 12$, $-14 \le k \le 14$, $-16 \le l \le 16$	$-16 \le h \le 17$, $-18 \le k \le 15$, $-16 \le l \le 19$	$-11 \le h \le 10$, $-20 \le k \le 19$, $-20 \le l \le 20$	$-41 \le h \le 48$, $-11 \le k \le 11$, $-17 \le l \le 15$	$-11 \le h \le 11$, $-19 \le k \le 14$, $-22 \le l \le 21$
ρ_{calcd} (Mg/m^3)	1697	1.824	1.771	1.676	1.680	1.858	1.718	1.904
abs. coeff (mm^{-1})	5.524	6.919	6.719	6.710	6.528	8.395	7.762	8.956
θ range (deg)	1.74–27.50	1.53–27.50	0.74–25.00	1.76–27.50	1.54–27.50	1.84–27.48	1.84–27.49	1.82–27.48
F(000)	1372	1160	2320	614	1400	1188	2376	1258
total no. of rflns	18 856	28 853	25 213	13 423	19 808	15 451	31 783	15 739
no. of indep rflns	6319 (R(int) = 0.0529)	10 044 (R(int) = 0.0337)	7952 (R(int) = 0.0670)	5778(R(int) = 0.0294)	6471 (R(int) = 0.0328)	5017 (R(int) = 0.0477)	9719 (R(int) = 0.0652)	5205 (R(int) = 0.0343)
no. of params varied	343	532	532	304	295	223	433	232
final R indices ($I > 2\sigma(I)$)[b]	R1 = 0.0440, wR2 = 0.1186	R1 = 0.0286, wR2 = 0.0686	R1 = 0.0631, wR2 = 0.1478	R1 = 0.0379, wR2 = 0.1012	R1 = 0.0343, wR2 = 0.0910	R1 = 0.0452, wR2 = 0.1089	R1 = 0.0571, wR2 = 0.1120	R1 = 0.0325, wR2 = 0.0727
R indices (all data)	R1 = 0.0584, wR2 = 0.1254	R1 = 0.0343, wR2 = 0.0710	R1 = 0.0828, wR2 = 0.1596	R1 = 0.0462, wR2 = 0.1054	R1 = 0.0427, wR2 = 0.0951	R1 = 0.0614, wR2 = 0.1156	R1 = 0.1017, wR2 = 0.1254	R1 = 0.0412, wR2 = 0.0755
goodness of fit on F^2 (GOF)[c]	1.081	1.031	1.150	1.042	1.051	1.035	1.016	1.085
largest diff peak and hole (e Å^{-3})	2.416 and −1.444	1.739 and −0.734	1.492 and −1.388	1.932 and −0.525	1.961 and −1.448	2.576 and −1.082	1.096 and −0.981	1.375 and −0.896

[a] For all crystal determinations, the scan type and wavelength of radiation used are ω and 0.710 73 Å, respectively. [b] $R1 = (\sum||F_o| - |F_c||)/(\sum|F_o|)$; $wR2 = [\sum(F_o^2 - F_c^2)/\sum(F_o^2)]^{1/2}$. [c] $GOF = [\sum w(F_o^2 - F_c^2)^2/(n - p)]^{1/2}$.

Scheme 2

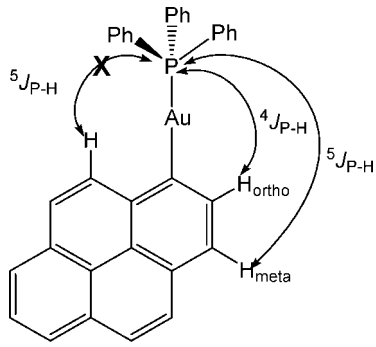

The X-ray intensity data were measured on a Bruker AXS SMART CCD three-circle diffractometer using graphite-monochromated Mo Kα radiation (λ = 0.710 73 Å) by a $2\theta-\omega$ scan. The software used was SMART[20a] for collecting frames of data, indexing reflection, and determination of lattice parameters, SAINT[20a] for integration of intensity of reflections and scaling, SADABS[20b] for empirical absorption correction, and SHELXTL[20c] for space group determination, structure solution, and least-squares refinements on $|F|^2$. Positional and anisotropic atomic displacement parameters were refined for all non-hydrogen atoms. The hydrogen atoms were placed in their ideal positions. Restraints (DFIX[20c] for C−C bonds and ISOR[20c] for thermal parameters) were applied during final refinement cycles for the ethyl groups of **9**. Some restraints on bond lengths and thermal parameters were also applied to the ethyl groups of **7**. Crystallographic data and experimental details are given in Table 1.

Results and Discussion

Synthesis of Aurated Pyrenes. The bromopyrenes were lithiated by reacting bromopyrenes with a slight excess of *n*-BuLi. Subsequent reactions of the lithiated pyrene with Au(PPh$_3$)Cl resulted in the formation of the monoaurated (**1**) and diaurated (**2**−**4**) pyrene complexes in reasonable to good yields of 53–86% (Scheme 1). Interestingly, reacting Au(PPh$_3$)Cl with lithiated 1,3,6-tribromopyrene only gave the diaurated complex **4** as the only product. The auration only occurred at the C1 and C6 positions; the Br at the C3 position remained unreacted. This result suggested that lithiation of 1,3,6-tribromopyrene is regioselective and is restricted to the C1 and C6 positions. A possible explanation is that the two negative charges are most widely separated when they reside on C1 and C6 (cf. C1 and C3, and C3 and C6), and this contributes to the stability of the lithiated intermediate. Further lithiation and auration of **4** to produce a trinuclear complex were not successful. Possibly, addition of an AuPPh$_3$ group at C3 is sterically hindered by the existing AuPPh$_3$ group at C1.

The $^{31}P\{^1H\}$ NMR spectra of **1**–**3** all show a singlet at δ ~45 ppm. This is indicative of the expected symmetry for **2** and **3** rendering the two AuPPh$_3$ groups equivalent. For **4**, two singlets of equal intensity were observed at δ ~44.94 and 44.44 ppm, respectively, and this is in agreement with the fact that the two AuPPh$_3$ groups at C1 and C6 are chemically inequivalent. The ^{1}H NMR spectra of **1**−**4** showed long-range P−H couplings between the P atom and the H atoms ortho ($^4J_{H-P}$) or meta ($^5J_{H-P}$) to the Au atom with $^4J_{P-H}$ = 5 Hz and $^5J_{P-H}$ = 1 Hz (Scheme 2 and SF1). The P−H couplings were confirmed by TOCSY experiments (SF2), which indicated that these couplings were not long-range H−H couplings. Interestingly, no $^5J_{P-H}$ coupling was observed between the P atom and the H atom on a different six-membered ring. To the best of our knowledge, no such long-range P−H coupling was reported before in the literature for arylgold(I) phosphines.

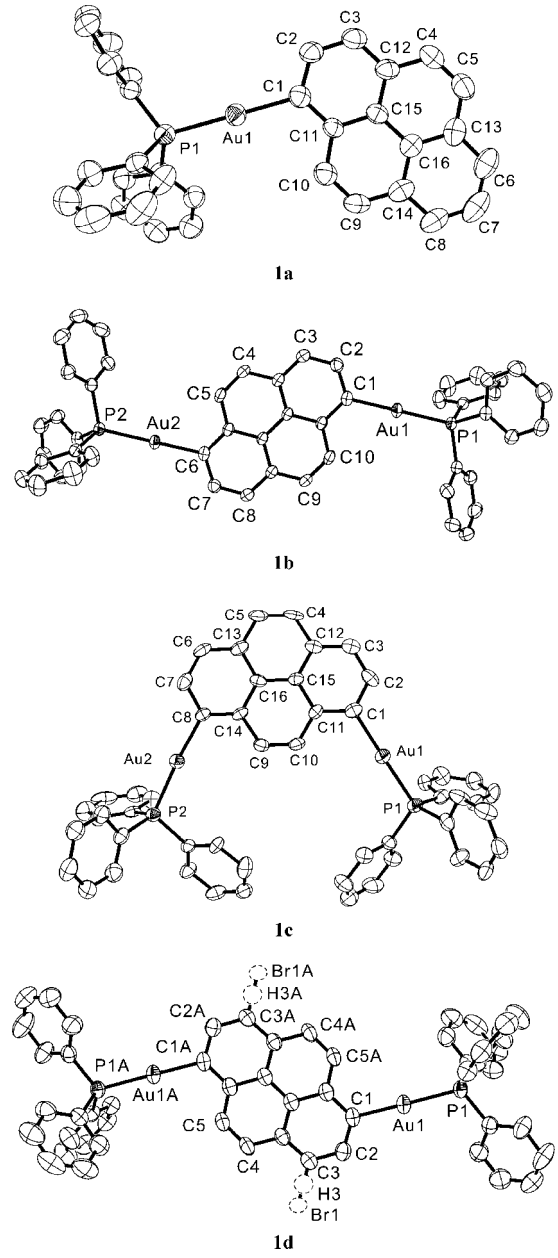

Figure 1. ORTEP diagrams of **1**·0.5CH_2Cl_2 (**1a**), **2**·CH_2Cl_2 (**1b**), **3**·CH_2Cl_2 (**1c**), and **4**·Et_2O (**1d**). All H atoms and solvent molecules are omitted for clarity. Thermal ellipsoids are shown at the 50% probability level.

Table 2. Selected Bond Lengths (Å) and Angles (deg) of 1–4

	1	2	3	4
Au1−C1	2.053(6)	2.042(3)	2.033(11)	2.051(5)
Au1−P1	2.2943(5)	2.2820(9)	2.282(3)	2.2901(14)
Au2−C6/C8		2.050(3)	2.065(12)	
Au2−P2		2.3001(9)	2.285(3)	
C1−Au1−P1	177.11(16)	179.14(11)	173.4(3)	179.04(17)
P2−Au2−C6/C8		172.78(10)	175.1(3)	

Structures of Aurated Pyrenes. Parts a−d of Figures 1 display the crystal structures of **1**·0.5 CH_2Cl_2, **2**·CH_2Cl_2, **3**·CH_2Cl_2, and **4**·Et_2O, respectively, and selected bond lengths and angles are given in Table 2. The Au ions in all the complexes are two-coordinated with a linear geometry. All complexes are monomeric with no discernible aurophilic

interactions and $\pi-\pi$ stacking of pyrenyl rings. The potential aggregation of the molecules could be hindered by the bulky PPh_3 ligands. The Au−C bond lengths span from 2.033(11) to 2.065(12) Å and the Au−P bond lengths from 2.2820(9) to 2.3001(9) Å; the C−Au−P bond angles are close to linearity, ranging from 172.78(10) to 179.04(17)°. These values are typical for known arylgold(I) complexes.[12,14–16] Complexes **3** and **5** show approximate C_{2h} and C_{2v} symmetry, respectively. The structure of complex **4** shows a Br atom at C3 and two $AuPPh_3$ groups at C1 and C6. The Br atom is disordered over two positions (C3 and C3A, 50% occupancy at both positions), which are related by an inversion center.

Synthesis of Platinated Pyrenes. Oxidative addition of excess $Pt(PEt_3)_4$ to the bromopyrenes in toluene resulted in the formation of the platinated pyrenyl complexes **5–9** in mostly good yields (Scheme 1). The platination of 1-bromopyrene and 1,6-/1,8-dibromopyrene gave a single product, as expected. However, the reaction of 1,3,6-tribromopyrene produced two geometrical isomers, 1,6-bis[*trans*-$Pt(PEt_3)_2Br$]-3-bromopyrene (**8**) and 1,8-bis[*trans*-$Pt(PEt_3)_2Br$]-3-bromopyrene (**9**), in approximately a 1:1 ratio. Only two out of the three Br atoms could be replaced by Pt ions for 1,3,6-tribromopyrene, even with excess $Pt(PEt_3)_4$. The Br at the C3 remained unreacted. This could be due to the presence of the bulky $Pt(PEt_3)_2Br$ group at the position meta to the remaining C−Br bond, which hinders the approach of another $Pt(PEt_3)_4$.

Complexes **5–7** display a singlet with Pt satellites in their respective $^{31}P\{^1H\}$ NMR spectra. On the other hand, two singlets with equal intensity at $\delta \sim 12$ ppm were observed in the spectra of **8** and **9**. The magnitude of $^1J_{P-Pt}$ (2680–2730 Hz) is consistent with the trans orientation of the two PEt_3 groups in the complexes. Interestingly, no long-range P−H coupling, as observed in the spectra of the gold complexes, was found in the spectra of the Pt complexes. This suggests that the P−H coupling is sensitive to the orientation of the P atoms with respect to the pyrenyl ring in the Au and Pt complexes (see the following section).

Structures of the Platinated Pyrenes. Parts a−d of Figures 2 show the crystal structures of **5**−**8**, and Table 3 gives the selected bond lengths and angles. The Pt ions in all complexes show distorted-square-planar geometry, and the coordination planes are nearly perpendicular to the pyrenyl rings with the angles between the two planes ranging from 79.4 to 89.8°. Complexes **6** and **7** show approximate C_{2h} and C_{2v} symmetry, respectively. The Br(2) atom in **8** is disordered over two positions which are related by an inversion center. The Pt−C (2.027(5)–2.047(9) Å) and Pt−P (2.30019(2)−2.3065(2) Å) bond lengths are normal.[15] The Pt−Br bonds (2.5050(6)–2.5258(9) Å) are longer than that in $PtBr_4^{2-}$ (2.446(6) Å),[21] probably due to the trans influence of the carbanion. Due to the motions of its ethyl groups, complex **7** showed large thermal parameters, and consequently the Pt−C bond length of the complex was not determined accurately. Despite many attempts, we failed to obtain good-quality crystals of **9**. Nevertheless, the crystal structure of the complex **9** (SF3) clearly showed the presence of two $Pt(PEt_3)_2Br$ groups at C1 and C8 and one Br atom at C3

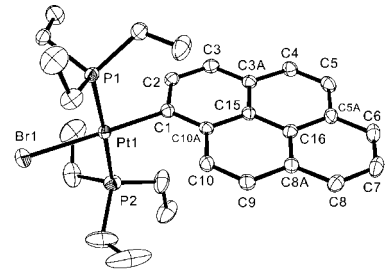

2a

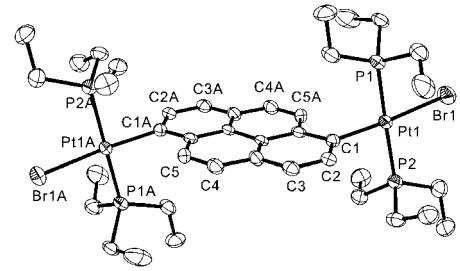

2b

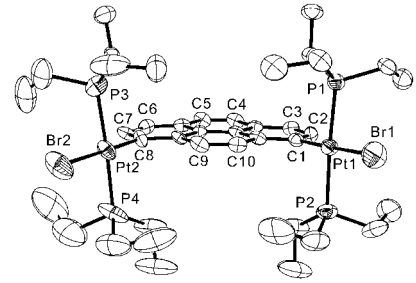

2c

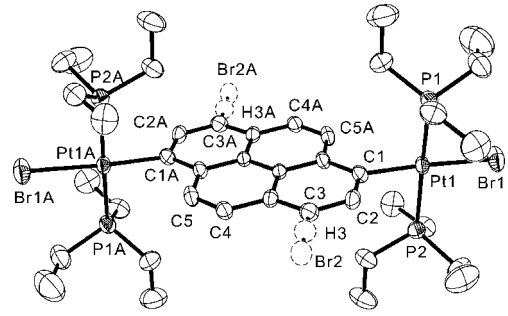

2d

Figure 2. ORTEP diagrams of **5** (**2a**), **6** (**2b**), **7** (**2c**), and **8** (**2d**). All H atoms are omitted for clarity. Thermal ellipsoids of **5** are shown at the 30% probability level, and those of **6–8** are shown at the 50% level.

Table 3. Selected Bond Lengths (Å) and Angles (deg) of 5–8

	5	6	7	8
Pt1−C1	2.027(5)	2.049(7)	2.001(11)	2.034(5)
Pt1−P1	2.3001(15)	2.3065(18)	2.295(3)	2.3027(14)
Pt1−P2	2.3015(12)	2.2994(19)	2.287(3)	2.3031(13)
Pt1−Br1	2.5050(6)	2.5258(9)	2.5007(18)	2.5117(6)
Pt2−C8			2.009(9)	
Pt2−P3			2.283(4)	
Pt2−P4			2.283(4)	
Pt2−Br2			2.5267(13)	
P1−Pt1−P2	177.13(5)	172.84(7)	176.33(13)	173.92(5)
C1−Pt1−Br1	177.21(13)	176.15(18)	177.4(3)	176.36(13)
P3−Pt2−P4			176.7(2)	
C8−Pt2−Br2			179.8(3)	

and a perpendicular orientation of the groups with respect to the plane of the pyrenyl ring.

(20) (a) *SMART & SAINT Software Reference Manuals, Version 4.0;*Siemens Energy & Automation, Inc., Analytical Instrumentation: Madison, WI, 1996. (b) Sheldrick, G. M. *SADABS: a Software for Empirical Absorption Correction*; University of Gottingen: Gottingen, Germany, 1996. (c) *SHELXTL Reference Manual, Version 5.03*; Siemens Energy & Automation, Inc., Analytical Instrumentation: Madison, WI, 1996.

(21) Kroening, R. F.; Rush, R. M.; Martin, D. S., Jr.; Clardy, J. C *Inorg. Chem.* **1974**, *13*, 1366.

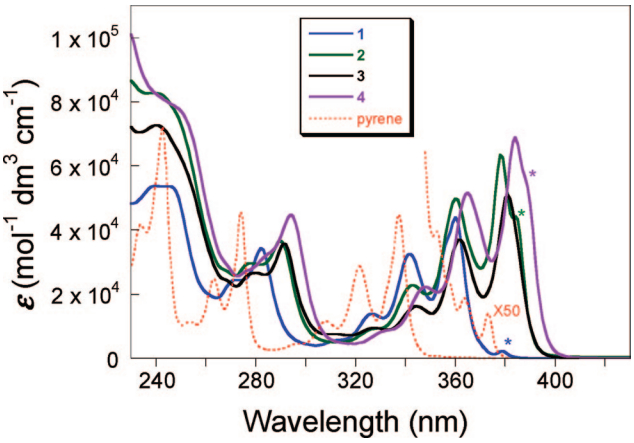

Figure 3. UV–vis absorption spectra of the gold complexes **1**–**4** and pyrene in CH_2Cl_2 at 295 K. The asterisks indicate the $^1\mathbf{L_b}$ bands.

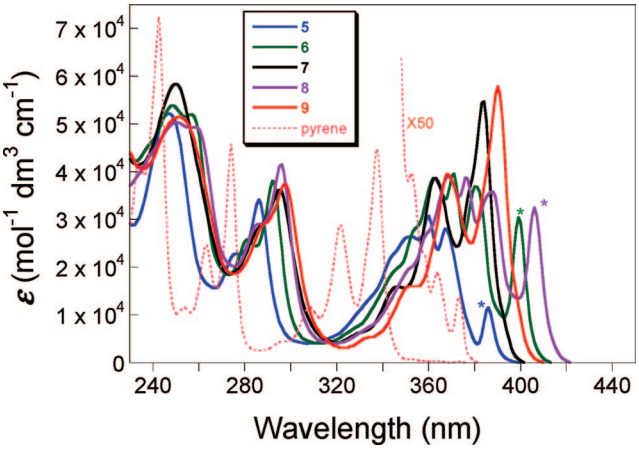

Figure 4. UV–vis absorption spectra of the gold complexes **5**–**9** and pyrene in CH_2Cl_2 at 295 K. The asterisks indicate the $^1\mathbf{L_b}$ bands of **5**, **6**, and **8**, respectively.

Table 4. Absorption and Emission Data of 1–9

complex	$^1\mathbf{L_a}$ (nm)[a]	$^1\mathbf{L_b}$ (nm)	$^1\mathbf{B_a}$ (nm)	$^1\mathbf{B_b}$ (nm)	λ_f (nm)[b]	λ_p (nm)[c]	$10^3\Phi_f$	$10^3\Phi_p$
1	360	378	240	282	*e*	605	*e*	~1
2	378	385	240	289	398	619	9.90	3.90
3	382	*d*	240	292	395	613	61.00	0.72
4	384	*d*	~250	294	416	630	0.67	2.60
5	367	386	247	286	397	608	0.87	1.17
6	381	400	249	292	412	625	0.50	2.88
7	383	*d*	250	295	406	626	2.72	0.80
8	388	406	250	296	419	634	0.42	2.31
9	390	*d*	252	298	417	635	1.17	0.62

[a] Positions of the lowest energy vibronic peak of the $^1\mathbf{L_a}$ band. [b] Fluorescence maxima. [c] Phosphorescence maxima. [d] tThe ^1L_b band merges with the $^1\mathbf{L_a}$ band. [e] Cannot be determined accurately.

Absorption Spectroscopy. The UV–vis absorption spectra of the complexes are dominated by intraligand $\pi \rightarrow \pi^*$ transitions of their pyrenyl rings (see Figures 3 and 4 for the spectra of Au and Pt complexes, respectively, and Table 4 for the spectral data).

All the spectra display a very intense band in the UV region around 250 nm (extinction coefficient $\epsilon_{max} = 5-8 \times 10^4$ M^{-1} cm^{-1}), an intense band at 270–310 nm ($\epsilon_{max} = 3.4–4.5 \times 10^4$ M^{-1} cm^{-1}), and a vibronic band at 310–410 nm ($\epsilon_{max} = 4.4–6.8 \times 10^4$ M^{-1} cm^{-1}), which are assigned to the $^1\mathbf{B_a}$, $^1\mathbf{B_b}$, and $^1\mathbf{L_a}$ bands (see below for the origins of the bands).[2a–c,4] A sharp

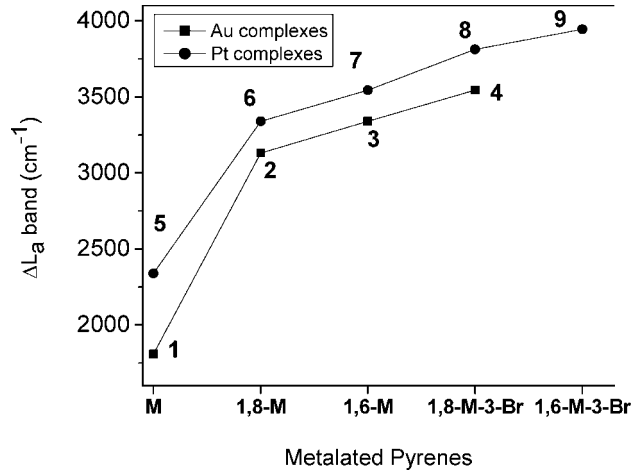

Figure 5. Plots of the red shifts of the $^1\mathbf{L_a}$ band of the Au and Pt complexes from that of pyrene versus the number and position of substitutions.

$^1\mathbf{L_b}$ band (378–406 nm) that is lower in energy than the $^1\mathbf{L_a}$ band is clearly observed in the spectra of **1**, **5**, **6**, and **8**, while in the spectra of **2** and **4**, the $^1\mathbf{L_b}$ band appears as a shoulder, as it overlaps with the $^1\mathbf{L_a}$ band. The $^1\mathbf{L_b}$ band completely merges with the $^1\mathbf{L_a}$ band in the spectra of **3**, **7**, and **9**. Because of the overlap, the I_1/I_2 ratios of the $^1\mathbf{L_a}$ band of **7** and **9** (~1.5) are higher than those of the other Pt complexes (~0.8) (I_1 and I_2 are the intensities of the first and second vibronic peaks of the $^1\mathbf{L_a}$ band).

The absorption bands of the complexes are all red-shifted from the corresponding absorptions of pyrene.[4,22] Plots of the $\Delta\mathbf{L_a}$ ($\Delta\mathbf{L_a}$ = energy difference between the ^1L_a bands of pyrene and substituted pyrene) (Figure 5) reveal several interesting features of the pyrenyl complexes. First, the effect of metal ions on the red shift is additive, as the extent of shift increases as the number of metal ions increases. Second, the perturbation of $AuPPh_3$ and $Pt(PEt_3)_2Br$ groups on the pyrenyl ring is stronger than that of the Br atom; e.g. the $^1\mathbf{L_a}$ band of 1,3,6-tribromopyrene is only red-shifted from that of pyrene by 2100 cm^{-1} in comparison with the 3945 cm^{-1} shift displayed by **9**. Third, the influence of the $Pt(PEt_3)_2Br$ group on the absorptions appears to be slightly stronger than that of the $AuPPh_3$ group; for instance, the energy of $^1\mathbf{L_a}$ band of **5** is lower than that of **1** by 530 cm^{-1}. Fourth, the energy of the $^1\mathbf{L_a}$ band is sensitive to the positions of metalation, as the $^1\mathbf{L_a}$ bands of the 1,6-metalated **3**, **7**, and **9** are lower than those of their corresponding 1,8-metalated isomers **2**, **6**, and **8**.

The $^1\mathbf{L_b}$ bands of the complexes ($\epsilon_{max} = 2.2-33 \times 10^3$ M^{-1} cm^{-1}) are far more intense than that of pyrene ($\epsilon_{max} = 500$ M^{-1} cm^{-1}). The four absorption bands of pyrene arise from the transitions from HOMO-1 and HOMO to LUMO and LUMO+1. In the D_{2h} symmetry of pyrene, the HOMO-1 → LUMO, HOMO → LUMO, HOMO → LUMO+1, and HOMO-1 → LUMO+1 excitations lead to the four singlet excited states $^1B_{3u}(1)$ $^1B_{2u}(1)$, $^1B_{3u}(2)$, and $^1B_{2u}(2)$, respectively.[1b,2a–c,23] The two $^1B_{3u}$ states are degenerate and would mix strongly via first-order configuration interactions, leading to a high-energy $^1B_{3u}{}^+$ state and a low-energy $^1B_{3u}{}^-$ state. The order of the energies of the four singlet excited states is $^1B_{3u}{}^-$ (^1L_b) < $^1B_{2u}$ (^1L_a) << $^1B_{3u}{}^+$ (^1B_b) < $^1B_{2u}$ (^1B_a) (shown in parentheses are

(22) (a) Clar, E. *Spectrochim. Acta* **1950**, *4*, 116. (b) Yoshinaga, T.; Hiratsuka, H.; Tanzaki, Y. *Bull. Chem. Soc. Jpn.* **1977**, *50*, 3096.
(23) Platt, J. R. *J. Chem. Phys.* **1949**, *17*, 484.

Scheme 3

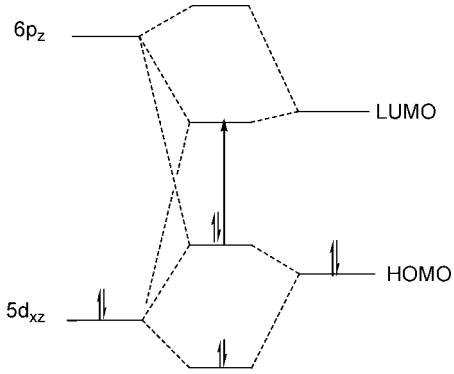

the labels of the excited states in Platt's nomenclature). The transitions from the S_0 ground state to the ^1L_b, ^1L_a, ^1B_b, and ^1B_a states lead to the $^1\mathbf{L_b}$, $^1\mathbf{L_a}$, $^1\mathbf{B_b}$, and $^1\mathbf{B_a}$ bands, respectively. Because the $S_0 \rightarrow {}^1L_b$ transition is pseudoparity forbidden,[24] the $^1\mathbf{L_b}$ band of pyrene is very weak. Attaching the Au and Pt groups to pyrene definitely relaxes the forbidden rule, as evidenced by the intense $^1\mathbf{L_b}$ bands of the complexes. Notably, the intensity of the $^1\mathbf{L_b}$ band increases more than 2-fold as the number of Pt ions increases from 1 to 2 ($\epsilon_{max} = 1.2 \times 10^4$ M^{-1} cm^{-1} for **5** and $\sim 3 \times 10^4$ M^{-1} cm^{-1} for **6** and **8**). It corroborates with the idea that the metal perturbation is additive.

The red shift of transitions and the intensification of the $^1\mathbf{L_b}$ band are due to perturbation of the metal ion on the pyrenyl ring. The $AuPPh_3$, $Pt(PEt_3)_2Br$, and Br groups can affect the ring via their inductive effects and through their orbital interactions with the ligand.[2] In a first-order approximation, the change in the energy of a molecular orbital R (δE_R) due to inductive effect is related to the change in Coulomb integral ($\delta\alpha$) by the equation $\delta E_k = \sum_i c_{ik}^2 \delta\alpha_i$, where c_{ik} is the linear-combination-of-atomic-orbital (LCAO) coefficient of the $2p_z$ orbital of the substituted carbon atom i in molecular orbital k.[3b] Semiempirical calculation on pyrene shows that the LCAO coefficients for the $2p_z$ orbitals of C1/3/6/8 in the HOMO (0.346) and LUMO (0.348) are nearly the same (SF4 and ST1). Accordingly, $\delta E_{HOMO} \approx \delta E_{LUMO}$. It is therefore unlikely that the red shifts of the absorption bands, especially the $^1\mathbf{L_a}$ band, are due to the inductive effect alone. Orbital interactions between the metal ions and pyrene mainly involve the metal dπ orbitals and the HOMO and LUMO of the ring. As the lowest energy absorption is ligand-centered, it is reasonable to assume that the metal dπ orbitals are lower in energy than the HOMO. Since the dπ orbitals are closer in energy to the HOMO than to the LUMO, the HOMO should be more destabilized than the LUMO by the metal π donation.[25] On the other hand, the $6p_z$ orbital of the metal ion is closer in energy to the LUMO than to the HOMO, and accordingly interactions of these orbitals would stabilize the LUMO more than the HOMO. Scheme 3 depicts a qualitative orbital interaction diagram for the metalated pyrenes. The overall result is a smaller HOMO–LUMO gap and red shift of the absorptions. The spectroscopic results showed that the $Pt(PEt_3)_2Br$ group is slightly stronger than the $AuPPh_3$ group in term of perturbation on the pyrenyl ring. This could be due to the fact the $Pt(PEt_3)_2Br$ group with its strongly electron-donating PEt_3 is a better π donor than the $AuPPh_3$ group.

Another consequence of the metal–ligand interactions is that the mixing of metal and ligand orbitals lowers the local D_{2h} symmetry of the pyrenyl ring. As a result, the degeneracy of the two $^1B_{3u}$ states is removed and the $^1A_g \rightarrow {}^1B_{3u}^-$ ($S_0 \rightarrow {}^1L_b$) transition is no longer forbidden.

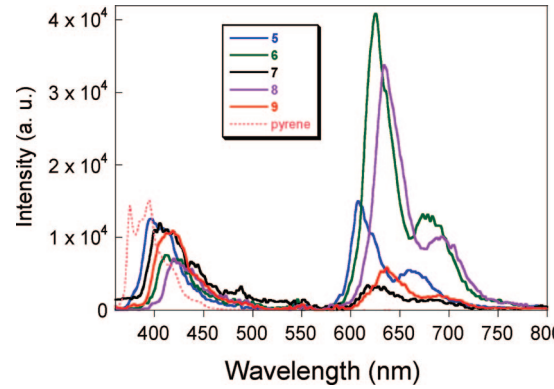

Figure 6. Emission spectra of **5–9** and pyrene in degassed CH_2Cl_2. $\lambda_{ex} = 320$ nm.

It is interesting to find that the energy gap between the $^1\mathbf{L_a}$ and $^1\mathbf{L_b}$ bands is sensitive to the position of metalation. The peak-to-peak separation of the two bands in pyrene is 1400 cm^{-1}. Similar separation is found in **1** (1300 cm^{-1}). On the other hand, the bands partially overlap in the 1,6-diaurated complexes **2** and **4** and merge in the 1,8-diaurated complex **3**. The bands are separated by $\sim$1200 cm^{-1} in **5**, **6**, and **8**. Similar to the case for their gold analogues, these bands completely overlap in the 1,8-diplatinated complexes **7** and **9**. As discussed in the next section, this variation of $^1\mathbf{L_a}$–$^1\mathbf{L_b}$ band gap could have a significant effect on the emissions of the complexes.

Emission Spectroscopy. All the pyrenyl complexes are luminescent in the solid state and solution. The emission quantum yields are given in Table 4. The solid-state emission spectra of **1–9** display intense fluorescence at 360–500 nm and weak phosphorescence at 600–750 nm (SF5). The gold complexes are unstable in solution and slowly decompose to pyrene and colloidal gold. A CH_2Cl_2 solution of **1** showed an intense 375 nm emission of pyrene[4] within 20 min after preparation. Because pyrene is much more emissive than the gold complex (fluorescence quantum yield $\Phi_f = 0.4$),[4] the emission spectrum of **1** was dominated by the fluorescence of pyrene. Nonetheless, the extent of decomposition was small for freshly prepared solution, as its UV–vis spectrum did not show any peaks ascribable to pyrene (see Figure 3) and weak phosphorescence at 600−750 nm arising from the Au complex was observed (phosphorescence quantum yield $\Phi_p \approx 0.001$). Changing the solvent to THF did not stop the decomposition.

Complexes **2**−**4** are more stable and display fluorescence and phosphorescence in degassed CH_2Cl_2 solutions (SF6). The phosphorescence of the 1,6-diaurated **2** ($\Phi_p = 3.9 \times 10^{-3}$) and **4** ($\Phi_p = 2.6 \times 10^{-3}$) is stronger than that of **1**. Surprisingly, the Φ_p value of the 1,8-diaurated **3** (7.2×10^{-4}) is the lowest among all the Au complexes.

The platinum complexes **5–9** are stable in solution, and emission spectra of degassed CH_2Cl_2 solutions of the compounds are shown in Figure 6.

Photoexcitation of degassed CH_2Cl_2 solutions of **5–9** at 350 nm caused fluorescence at 370–500 nm and vibronic phosphorescence at 600–750 nm. As with the electronic absorption spectra, the more atoms substituted on pyrene, the more red-shifted the fluorescence band became. It is noted that the Φ_p value increases only in the series **5** < **6** < **8** involving the 1,6-platinated complexes. Analogous to the Au counterparts, the Φ_p values of 1,8-platinated **7** and **9** are lower than for the 1,6-

(24) Pariser, R. *J. Chem. Phys.* **1956**, *24*, 250.
(25) Creutz, C.; Newton, M. D.; Sutin, N. *J. Photochem. Photobiol. A* **1994**, *82*, 47.

diplatinated complexes and even the monoplatinated complex **1**. While pyrene is known to exhibit excimeric emission around 460 nm at high concentration,[2a–c] no such emission was observed in the spectra of the complexes even at a concentration of 10^{-4} M.

The fluorescence of pyrene and substituted pyrenes mainly arises from radiative decay of the lowest energy singlet excited state ^1L_b. Intersystem crossing from the ^1L_b state to its corresponding triplet ^3L_b state, probably mediated by another triplet state, gives rise to the phosphorescence.[26] Because of the unfavorable Franck–Condon factor and the spin-forbidden nature of the intersystem crossing, phosphorescence of pyrene has not been observed under normal circumstances. With their strong spin–orbit coupling, the Au and Pt ions could facilitate the intersystem crossing by mixing the spin parentages of the states. Indeed, the metalated pyrenes display phosphorescence, indicating the presence of an intramolecular heavy atom effect in the complexes. The effect is particularly obvious for the Pt complexes, in which an increase in the Φ_p value is accompanied by a decrease in the Φ_f value.

Expectedly, the Φ_p value of the dimetalated complexes is higher than that of the mononuclear complexes. However, all 1,8-dimetalated complexes show anomalously low Φ_p values. This could be related to the complete overlap of the $^1\mathbf{L_a}$ and $^1\mathbf{L_b}$ bands of the complexes, which implies a close proximity of the ^1L_a and ^1L_b states. A fast equilibrium between the states would reduce the population of the ^1L_b state and, hence, the ^3L_b state. In other words, formation of the ^1L_a state and its subsequent decays compete with the intersystem crossing from ^1L_b to ^3L_b and thus reduce the Φ_p value.

(26) (a) Barradas, I.; Ferreira, J. A.; Thomaz, M. F. *J. Chem. Soc., Faraday Trans. 2* **1973**, 388. (b) Jones, P. F.; Siegel, S. *Chem. Phys. Lett.* **1968**, *2*, 486. (c) Shimizu, Y.; Azumi, T. *J. Phys. Chem.* **1982**, *86*, 22.

Conclusion

In this work, nine new gold and platinum complexes of pyrene have been synthesized. Our study showed that it is not possible to attach more than two $AuPPh_3$ and $Pt(PEt_3)_2Br$ units to the rim of pyrene. The electronic spectroscopy of the complexes demonstrated the perturbation of metal ions on the electronic structures of the pyrenyl ring. The perturbation causes red shifts of the $\pi \rightarrow \pi^*$ absorptions and intensifies the otherwise forbidden $^1S_0 \rightarrow {}^1L_b$ transition. The energy gap between the ^1L_a and ^1L_b states can be varied by changing the number and position of the metal ion in the ring. The small ^1L_a–^1L_b energy gap of the 1,8-dimetalated complexes is suggested to be the cause of their relatively weak phosphorescence.

Acknowledgment. The authors thank National University of Singapore for financial support and Ms. G. K. Tan and Professor Kop Lip Lin for assistance with the X-ray crystal structure determination.

Supporting Information Available: Figures and tables giving ^1H NMR and TOCSY spectra of **4**, the crystal structure of **9**, molecular orbitals and LCAO coefficents of pyrene, solid-state emission spectra of **1**–**9**, and solution emission spectra of the gold complexes and CIF files giving crystal data for **1**−**9**. This material is available free of charge via the Internet at http://pubs.acs.org

OM700716P